Preparation and Swelling Characteristics of a Superabsorbent Nanocomposite Based on Natural Guar Gum and Cation-Modified Vermiculite

Wenbo Wang,[1,2] Naihua Zhai,[1,2] Aiqin Wang[1]

[1]*Center for Eco-Material and Green Chemistry, Lanzhou Institute of Chemical Physics, Chinese Academy of Sciences, Lanzhou 730000, China*
[2]*Graduate University of the Chinese Academy of Sciences, Beijing 100049, China*

Received 31 December 2009; accepted 17 July 2010
DOI 10.1002/app.33083
Published online 30 September 2010 in Wiley Online Library (wileyonlinelibrary.com).

ABSTRACT: A series of novel superabsorbent nanocomposites were prepared by the solution radical polymerization of natural guar gum (GG), partially neutralized acrylic acid [sodium acrylate (NaA)], and cation-exchanged vermiculite (M^{n+}-VMT) with ammonium persulfate as the initiator in the presence of the crosslinking agent *N,N′*-methylene-*bis*-acrylamide. Fourier transform infrared analysis revealed that NaA was grafted onto the GG chains and that M^{n+}-VMT participated in the polymerization. X-ray diffraction results showed that the occurrence of the cation-exchange process changed the interlayer gap of vermiculite (VMT) and that M^{n+}-VMT was exfoliated during polymerization to form a nanocomposite. The exfoliated VMT led to better dispersion in the GG-*g*-poly(sodium acrylate) matrix, as shown by scanning electron microscopy and transmission electron microscopy analysis. M^{n+}-VMT improved the water absorption of the nanocomposite more remarkably than raw VMT, and Al^{3+}-VMT enhanced the water absorption to the highest degree. The nanocomposite exhibited intriguing overshooting swelling characteristics in a multivalent saline solution and acidic pH solution and showed switching pH-responsive behaviors in buffer solutions between pH 2 and pH 7.2. © 2010 Wiley Periodicals, Inc. J Appl Polym Sci 119: 3675–3686, 2011

Key words: guar gum; vermiculite; superabsorbent nanocomposite; pH-sensitive; swelling

INTRODUCTION

Polymer/clay nanocomposites have long been an attractive subject for scientific research and industrial application because the combination of clay mineral with organic polymer can obviously reduce the production cost and improve the performance of materials.[1–3] *Superabsorbents* are moderately crosslinked three-dimensional hydrophilic polymer networks that can absorb and retain large amounts of aqueous solutions compared with general absorbents. Because of the unique properties, superabsorbents have found extensive applications in various fields, including agriculture,[4,5] hygienic products,[6] cosmetics,[7] wastewater treatment,[8,9] and drug-delivery systems.[10,11] Recently, many kinds of materials have been used to develop superabsorbents to improve their performance and extend their applications.[12–17] Among them, composites of low cost, annually renewable and biodegradable polysaccharides with abundant inorganic clays, and their substitutes for petroleum-based polymers have attracted considerable attention because they offer both commercial and environmental advantages.[18]

Guar gum (GG) derived from the seeds of the guar plant *Cyanaposis tetragonolobus* (Leguminosae) is a nonionic branched polymer with β-D-mannopyranosyl units linked (1–4) with single membered α-D-galactopyranosyl units occurring as side branches. GG and its derivatives have been used in many areas (e.g., thickening agents, suspending agents, ion-exchange resins). Vermiculite (VMT) is a layered aluminum silicate with exchangeable cations (Scheme 1). The properties of traditional superabsorbents can be enhanced by the incorporation of raw VMT.[19] According to a previous description,[20] the performance of composite materials can be further improved through the modification of clay because moderate pretreatment can improve its compatibility with an organic matrix. As a popular, effective, and relatively facile method for the modification of clays, the ion-exchange process may induce

Correspondence to: A. Wang (aqwang@licp.cas.cn).
Contract grant sponsor: West Light Foundation and the Western Action Project of Chinese Academy of Sciences; contract grant number: KGCX2-YW-501.
Contract grant sponsor: "863" Project of the Ministry of Science and Technology, People's Republic of China; contract grant numbers: 2006AA03Z0454, X2006AA100215.

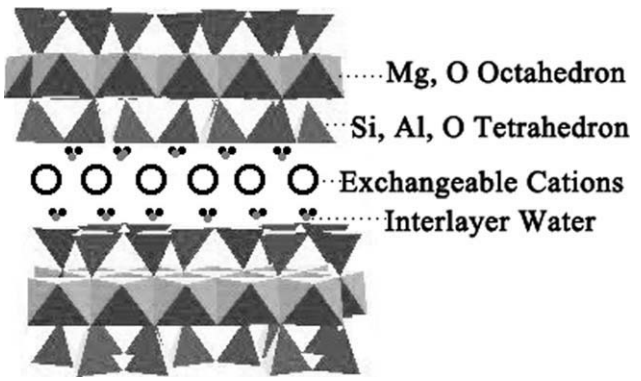

Scheme 1 Schematic structure of VMT.

enormous changes in the microscopic structures of clays.[21] In this study, we directed much attention toward the cation-exchange modification of raw VMT and its use as a functional filler. We expected that the type and amount of hydrophilic groups and the network structure of superabsorbents would be improved by the introduction of GG and cation-exchanged vermiculite (M^{n+}-VMT) synchronously.

On basis of the previous background, in this study, we prepared novel GG-*g*-poly(sodium acrylate) (PNaA)/M^{n+}-VMT superabsorbent nanocomposites from GG, sodium acrylate (NaA), and M^{n+}-VMT. Their structure and morphology was characterized by Fourier transform infrared (FTIR) spectroscopy, X-ray diffraction (XRD), and scanning electron microscopy (SEM). The swelling properties of the developed nanocomposites in various swelling media were also evaluated systematically.

EXPERIMENTAL

Materials

GG (food grade, number-average molecular weight = 220,000) was purchased from Wuhan Tianyuan Biology Co. (Wuhan, China). Acrylic acid (AA; chemically pure, Shanghai Shanpu Chemical Factory, Shanghai, China) was distilled under reduced pressure before use. Unexpanded VMT (Linze Colloidal Co., Gansu, China) was milled and passed through a 320-mesh screen before use, and the capacity of exchangeable cations was 34.37 mmol/100 g. Ammonium persulfate (APS; analytical grade, Xi'an Chemical Reagent Factory, Xi'an, China) and *N*,*N*′-methylene-*bis*-acrylamide (MBA; chemically pure, Shanghai Chemical Reagent Corp., Shanghai, China) were used as purchased. The other reagents used were analytical grade, and all solutions were prepared with distilled water.

Preparation of the M^{n+}-VMT samples

VMT powder (particle size = 46 μm, 10.0 g) was suspended in 100 mL of 1 mol/L $MCl_n \cdot H_2O$ (where M is Li^+, Na^+, K^+, Mg^{2+}, Ca^{2+}, or Al^{3+}) solutions under vigorous stirring (1250 rpm) at room temperature for 4 h. The resulting M^{n+}-VMT (denoted as Li^+-VMT, Na^+-VMT, K^+-VMT, Mg^{2+}-VMT, Ca^{2+}-VMT, and Al^{3+}-VMT, respectively) was isolated from the suspension by centrifugation and washed with large amounts of distilled water to remove any impurities present and redundant saline until no Cl^- could be detected by a 0.1 mol/L $AgNO_3$ solution from the washed water. The M^{n+}-VMT was dried to a constant weight at 70°C and passed through a 320-mesh sieve (46 μm).

Preparation of the GG-*g*-PNaA/M^{n+}-VMT nanocomposites

GG powder (1.20 g) was dispersed in 34 mL of a 0.067 mol/L NaOH solution (pH 12.5) in a 250-mL, four-necked flask equipped with a mechanical stirrer, a reflux condenser, a thermometer, and a nitrogen line. The resulting dispersion was heated to 60°C with an oil bath and maintained for 1 h to form a colloidal slurry. Then, the aqueous solution of the initiator APS (4 mL, 0.1008 g) was dropped into the reaction flask under continuous mechanical stirring and maintained at 60°C for 10 min to generate radicals. AA (7.2 g) was neutralized with 8.5 mL of 8 mol/L NaOH until a total neutralization degree of 70% was reached (34 mL of the 0.067 mol/L NaOH solution used to disperse GG was considered as a part of the neutralization degree), and then, the crosslinker MBA (21.6 mg) and VMT micropowder (0.45 g) were charged into the neutralized AA solution under magnetic stirring. After the reactants were cooled to 40°C, this dispersion was added dropwise to the reaction flask, and the oil bath was slowly heated to 70°C and kept there for 3 h. A nitrogen atmosphere was maintained throughout the reaction period. The final gel products were dried to a constant weight at 70°C and then ground and passed through 40–80-mesh sieves (180–380 μm). The uncrosslinked PNaA and GG-*g*-PNaA were prepared by similar procedures except without the addition of VMT and MBA.

Measurements of the equilibrium water absorption and swelling kinetics

The dry sample (0.05 g) was immersed in excessive aqueous solution at room temperature for 4 h to reach swelling equilibrium. The swollen gels were separated from water with a mesh screen and then drained on the sieve for 10 min until no free water remained. After the swollen gels were weighed, the equilibrium water absorption was calculated by eq. (1):

$$Q_{eq} = (w_2 - w_1)/w_1 \quad (1)$$

where Q_{eq} is the equilibrium water absorption (g of water/g of sample) and w_1 and w_2 are the weights of the dry and water-swollen samples, respectively.

The swelling kinetics of superabsorbent in distilled water, saline solution, and various pH solutions were measured as follows: a certain amount of sample (ca. 0.05 g) was put in contact with 300-mL aqueous solution for a set interval (1, 3, 5, 8, 10, 20, 30, or 60 min), and then, the swollen gel was filtered with a sieve. A similar procedure was repeated for each time interval until the swelling equilibrium was reached. The water absorption at a given time was calculated according to eq. (1). The pH values of the external solutions were adjusted with standard 1 mol/L HCl or NaOH solution and measured with a pH meter (Mettler Toledo 320 pH meter, Zurich, Switzerland). In all cases, three parallel samples were used, and the averages are reported in this article.

Evaluation of the pH responsivity

Buffer solutions with various pH values were prepared by the proper combination of KH_2PO_4, K_2HPO_4, H_3PO_4, NaCl, and NaOH solutions. The ionic strengths of all of the buffer solutions were adjusted to 0.1*M* with an NaCl solution. The pH reversibility of the nanocomposite was investigated in terms of its swelling and deswelling between pH 2 and pH 7.2. Typically, the sample particle (0.05 g, 180–380 μm) was placed in a 100-mesh sieve and adequately contacted with 100 mmol/L pH 2.0 buffer solution until it reached equilibrium. Then, the swollen samples were soaked in pH 7.2 buffer solutions for set time intervals. The swollen samples were filtered and weighed, and then, we calculated the water absorption of the nanocomposite at a given moment according to the mass change of samples before and after swelling. The consecutive time interval was 18 min for each cycle, and the same procedure was repeated for four cycles. After every measurement, each solution was renewed.

Characterizations

FTIR spectra were recorded on a Nicolet NEXUS FTIR spectrometer (Madison Wisconsin, United States) in the 4000–400-cm^{-1} region with KBr platelets. The maximum absorption band of all of the samples was normalized as 10% (transmittance), the basic line was normalized as 100% (transmittance), and all of the FTIR data was analyzed by an OMNIC software pack. Thermal analysis of samples was carried out on a PerkinElmer TGA-7 thermogravimetric analyzer (PerkinElmer Cetus Instruments, Norwalk, CT, United States) in the temperature range 25–800°C at a heating rate of 10°C/min with a dry nitrogen purge at a flow rate of 50 mL/min. XRD analyses were performed with an X-ray power diffractometer with a Cu anode (PAN Analytical Col, X'pert PRO, ALMELO, The Netherlands) running at 40 kV and 30 mA and scanning from 3 to 10° at 3°/min. SEM studies were carried out in a JSM-5600LV SEM instrument (JEOL Ltd., Tokyo, Japan) after the sample was coated with gold film at an acceleration voltage of 20 kV. The Brunauer–Emmett–Teller (BET) specific surface area and average pore size of the samples were measured by an accelerated surface area and porosimetry system (Micromeritics, ASAP 2020, USA) by the BET method at 76 K.

RESULTS AND DISCUSSION

Superabsorbent composite networks could be formed by the simultaneous grafting and chemically crosslinking reaction of GG, NaA, MBA, and VMT (Scheme 2). At the initial stage, the initiator APS was decomposed under heating to generate sulfate anion radicals. Then, these radicals stripped down the hydrogen of —OH groups on GG to form alkoxy macroradicals. These macroradicals could act as the active sites during the reaction and could initiate NaA to process chain propagation.[22] During chain propagation, the crosslinker MBA, containing double vinyl groups, and VMT, containing active —OH groups, participated in the crosslinking reaction, and thus, a crosslinked network structure was formed.

FTIR and differential thermogravimetry analysis

The FTIR spectra of VMT and M^{n+}-VMT are shown in Figure 1(a–f). The —CH_3 and —CH_2 absorption bands of VMT at 2920 and 2845 cm^{-1} derived from the organic mineral congeries among VMT particles almost disappeared in the spectra of M^{n+}-VMT; this indicated that the mineral congeries were removed during treatment. The absorption band of VMT at 3668 cm^{-1} (asymmetrical stretching vibrations of —OH of silanol groups) and the absorption band at 915 cm^{-1} [stretching vibrations of Si—O(H)] were slightly strengthened after modification; this indicated that more Si—OH was exposed because of the removal of mineral congeries. The —OH stretching vibration bands of the interlayer H_2O molecules were 3446 cm^{-1} for raw VMT, 3431 cm^{-1} for Li^+-VMT, 3475 cm^{-1} for K^+-VMT, 3422 cm^{-1} for Mg^{2+}-VMT, 3434 cm^{-1} for Ca^{2+}-VMT, and 3430 cm^{-1} for Al^{3+}-VMT. The change order of these absorption bands was identical to the tendency reported in a previous report on M^{n+}-VMT;[23] this implied the occurrence of a cation-exchange reaction. This result was also proven by XRD analysis.

As shown in Figure 1(g–k), the characteristic absorption bands of GG at 1017, 1082, and 1158 cm^{-1} (stretching vibrations of C—OH) and the band

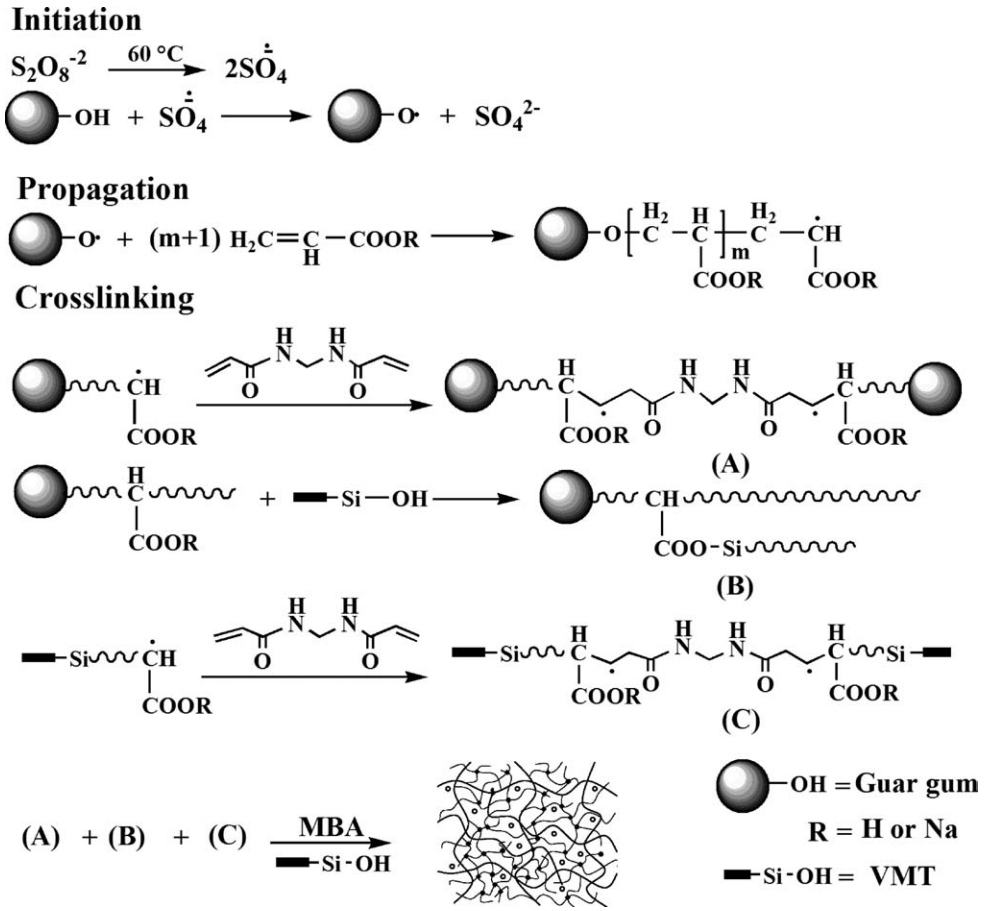

Scheme 2 Proposed mechanisms for the formation of the superabsorbent nanocomposite network.

at 1648 cm^{-1} (bending vibrations of —OH groups) were weakened after the reaction. New bands at 1565 cm^{-1} for GG-*g*-PNaA, 1569 cm^{-1} for GG-*g*-PNaA/K^+-VMT GG-*g*-PNaA/Mg^{2+}-VMT, 1571 cm^{-1} for GG-*g*-PNaA/Al^{3+}-VMT, and 1454 and 1410 cm^{-1} (asymmetric stretching and symmetric stretching in $—COO^-$ groups, respectively) appeared [Fig. 1(h–k)]. This result reveals that the PNaA chains existed in the superabsorbents, and the grating copolymerization reaction occurred among the GG macromolecular chains and NaA monomers. To confirm the grafting of NaA onto GG, the differential thermogravimetry curves of GG, uncrosslinked PNaA, and GG-*g*-PNaA polymers are presented (Fig. 2). The decomposition temperature and weight loss rate clearly changed after the graft reaction. GG, PNaA, and GG-*g*-PNaA showed one-step [peak maximum temperatures (T_{max}) = 308°C], three-step (T_{max} = 261, 398, and 447°C), and four-step (T_{max} = 244, 339, 397, and 436°C) thermal decompositions, respectively. After the graft polymerization reaction, the T_{max} of GG at 308°C shifted to 339°C, and the T_{max}'s of PNaA at 398 and 447°C shifted to 397 and 436°C, respectively. This indicated that NaA was grafted onto the GG backbone.[22] The (Si)O—H stretching vibration of VMT at 3668 cm^{-1} and the —OH bending vibration of M^{n+}-VMT at 1632 cm^{-1} almost disappeared after the reaction [Fig. 1(b–f,i–k)]. The absorption band of VMT at 998 cm^{-1}, attributed to ≡Si—O stretching, shifted to about 1012 cm^{-1} in the spectrum of the nanocomposite. This gave direct evidence that VMT participated in the graft copolymerization reaction through its active silanol groups.[24,25]

XRD analysis

The XRD patterns of VMT, Li^+-VMT, K^+-VMT, Mg^{2+}-VMT, Ca^{2+}-VMT, Al^{3+}-VMT, GG-*g*-PNaA/K^+-VMT (5 wt %), GG-*g*-PNaA/Mg^{2+}-VMT (5 wt %), and GG-*g*-PNaA/Al^{3+}-VMT (5 wt %) are shown in Figure 3. VMT showed a strong (001) reflection at 2θ = 7.17° with a basal spacing (*d*) of 1.23 nm [Fig. 2(a)]. After cation exchange, this reflection shifted to 2θ = 6.05° (*d* = 1.46 nm, Li^+-VMT), 2θ = 8.71° (*d* = 1.02 nm, K^+-VMT), 2θ = 6.17° (*d* = 1.43 nm, Mg^{2+}-VMT), 2θ = 6.00° (*d* = 1.47 nm, Ca^{2+}-VMT), and 2θ = 6.28° [*d* = 1.41 nm, Al^{3+}-VMT; Fig. 3(b–f)]; this indicated that cation exchange between the interlayer cations of VMT and the external cations occurred. Also, the VMT modified by different

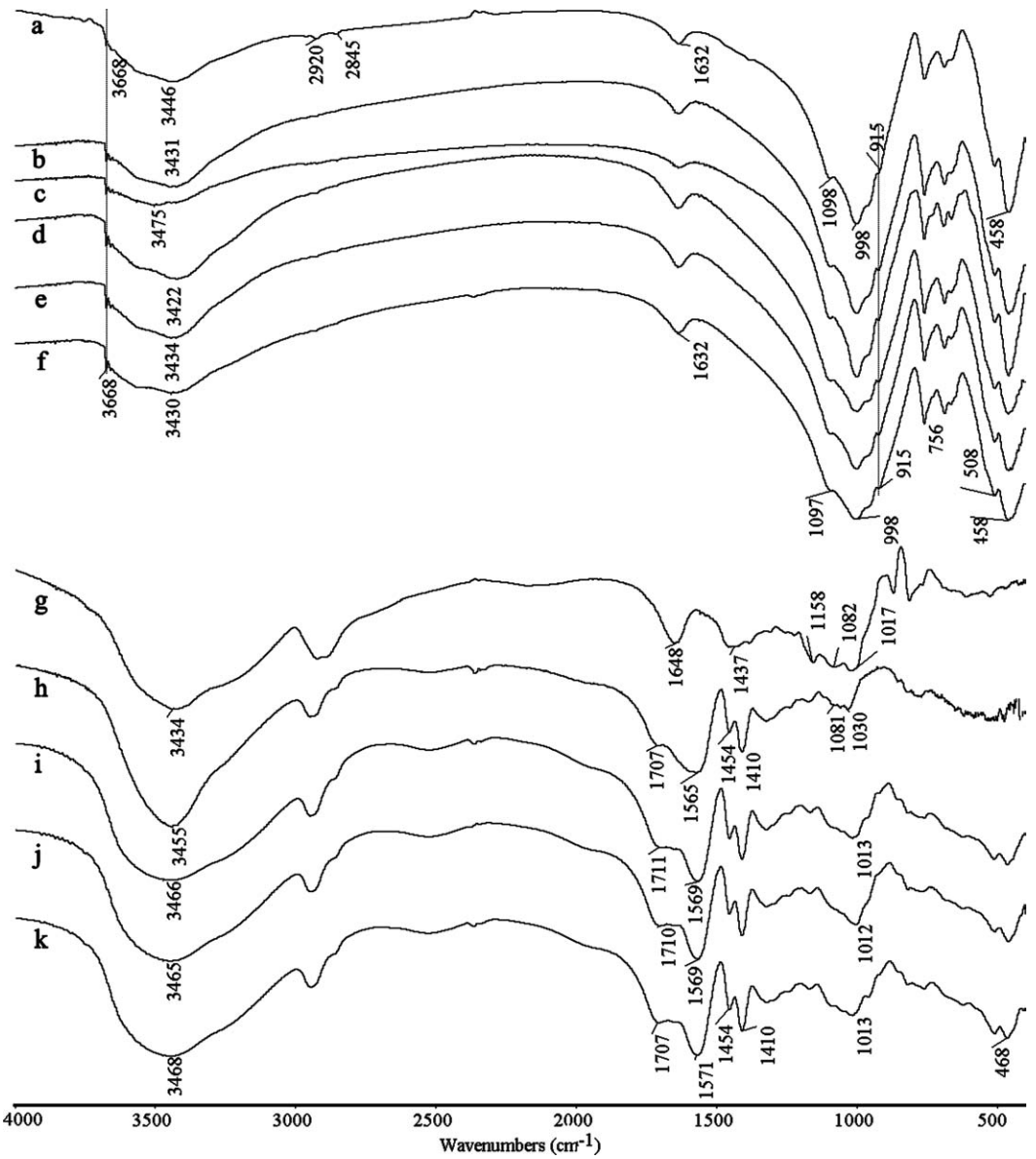

Figure 1 FTIR spectra of (a) VMT, (b) Li^+-VMT, (c) K^+-VMT, (d) Mg^{2+}-VMT, (e) Ca^{2+}-VMT, (f) Al^{3+}-VMT, (g) GG, (h) GG-*g*-PNaA, (i) GG-*g*-PNaA/K^+-VMT, (j) GG-*g*-PNaA/Mg^{2+}-VMT, and (k) GG-*g*-PNaA/Al^{3+}-VMT. The content of M^{n+}-VMT in the composite was 5 wt %.

cations showed distinct *d*-spacing: Ca^{2+}-VMT reached 1.47 nm, but K^+-VMT reached only 1.02 nm. This tendency was ascribed to the difference in the layer number of the interlayer water;[23] this resulted from the different ionic potentials of the cations. The ionic potentials of the cations increased in the order K^+ (7.52 nm^{-1}) < Na^+ (10.53 nm^{-1}) < Li^+ (14.71 nm^{-1}) < Ca^{2+} (20.20 nm^{-1}) < Mg^{2+} (30.77 nm^{-1}) < Al^{3+} (60.00 nm^{-1}). K^+-VMT presented the lowest layer number of interlayer water (0 layer) and the smallest *d* value. Li^+-VMT, Mg^{2+}-VMT, Ca^{2+}-VMT, and Al^{3+}-VMT presented two-layer interlayer water.[23] Because Ca^{2+} had a correspondingly greater ion radius than Mg^{2+} and Al^{3+} ions, it combined with water molecules for more relaxation and the greatest *d* value.

As shown in Figure 3(g–i), no diffraction peaks of VMT were observed in the XRD patterns of the composites. The absence of the characteristic reflections of M^{n+}-VMT in the composites revealed that VMT was almost exfoliated and was homogeneously dispersed in the polymer matrix.[26] Similar results were also observed in nanocomposite superabsorbent starch-grafted PAA-*co*-AM/MMT.[27]

SEM and transmission electron microscopy (TEM) analysis

Figure 4 shows the SEM micrographs of K^+-VMT, Mg^{2+}-VMT, Al^{3+}-VMT, the GG-*g*-PNaA hydrogel, and the superabsorbent nanocomposites. It was

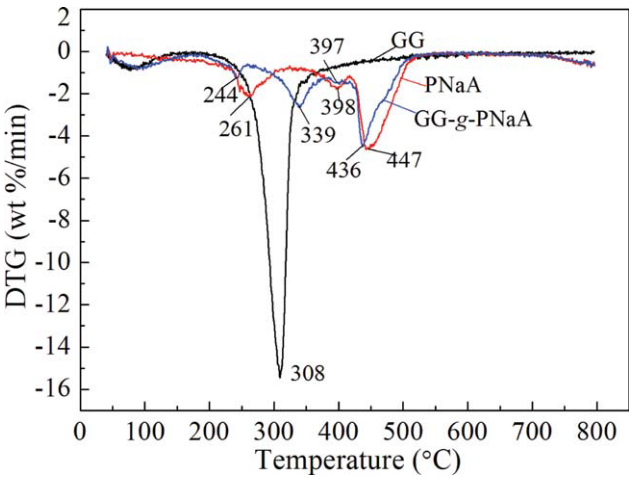

Figure 2 DTG curves of (a) GG, (b) uncrosslinked PNaA, and (c) uncrosslinked GG-*g*-PNaA. [Color figure can be viewed in the online issue, which is available at wiley onlinelibrary.com.]

evident that the VMTs modified by various cations showed similar morphologies, in which some sheet structures were observed. Also, GG-*g*-PNaA only showed a smooth and dense surface [Fig. 4(d)], whereas the nanocomposites all showed comparatively coarse and rough surfaces [Fig. 4(e–i)]. By comparing the micrographs shown in Figure 4(e–i), we observed that the nanocomposite derived from monovalent M^{n+}-VMT exhibited correspondingly course and porous surfaces compared to the multivalent ones. This phenomenon was ascribed to the additional surface crosslinking action of multivalent cations during polymerization. We also observed that the M^{n+}-VMT was almost embedded and uniformly dispersed within the GG-*g*-PNaA matrix [Fig. 4(e–i)]. The fine dispersion of VMT particles in the polymer matrix without flocculation facilitated the superabsorbent to form a homogeneous composition.

Figure 5 depicts the TEM image of the GG-*g*-PNaA/VMT superabsorbent nanocomposite. As shown, obvious VMT platelets were observed in the composite; this indicated that VMT led to a better dispersion in the polymeric matrix without flocculation. This observation was in accordance with the XRD and SEM results.

Effect of M^{n+}-VMT on the water absorption

Figure 6 shows the effects of M^{n+}-VMT on the water absorption in distilled water and 0.9 wt % NaCl solution. The nanocomposites improved the water absorption in the following order: VMT < Li^+-VMT < Na^+-VMT < K^+-VMT < Ca^{2+}-VMT < Mg^{2+}-VMT < Al^{3+}-VMT. Compared with VMT, M^{n+}-VMT improved the water absorption more remarkably, and the divalent (Ca^{2+} and Mg^{2+}) or trivalent cation (Al^{3+})-exchanged VMT enhanced the water absorption to a higher degree than the monovalent ones (Li^+, Na^+, and K^+). As described previously,[28] the exchange capability of VMT clay mineral with external cations followed the order Li^+ < Na^+ < K^+< Ca^{2+} < Mg^{2+} < Al^{3+}; this was consistent with the order of water absorption and revealed that cations with a strong exchange capability with VMT improved the water absorption more remarkably. To evaluate the changes in the physical parameters of VMT before and after modification, the BET specific surface area and average pore size were determined and are shown in Table I. The surface area of M^{n+}-VMT were all greater than that of VMT, and the exchange of Ca^{2+}, Mg^{2+}, and Al^{3+} increased the distribution of micropores or mesopores in VMT and enhanced the surface area of VMT to a greater degree than Li^+, Na^+, and K^+. Compared with VMT, these exchanged cations exhibited better arrangement in the clays.[29] These factors were favorable to the improvement of water absorption. In addition, the contribution of exchanged multivalent cations to the improvement of water absorption may have resulted from their complexation with hydrophilic groups (e.g., —COO^- and —OH), which acted as assistant crosslinking agents and facilitated the formation of a regular polymeric network.[30]

Effect of the Al^{3+} concentration on the water absorption

Al^{3+}-VMT improved the water absorption to the highest degree. The effect of the concentration of

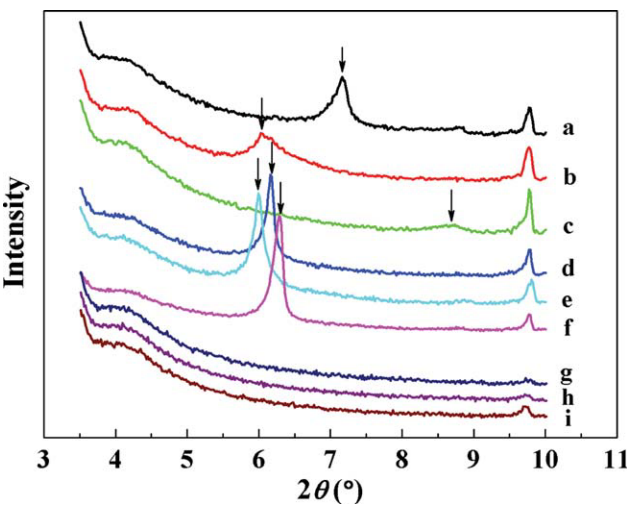

Figure 3 XRD patterns of (a) VMT, (b) Li^+-VMT, (c) K^+-VMT, (d) Mg^{2+}-VMT, (e) Ca^{2+}-VMT, (f) Al^{3+}-VMT, (g) GG-*g*-PNaA/K^+-VMT (5 wt %), (h) GG-*g*-PNaA/Mg^{2+}-VMT (5 wt %), and (i) GG-*g*-PNaA/Al^{3+}-VMT (5 wt %). [Color figure can be viewed in the online issue, which is available at wileyonlinelibrary.com.]

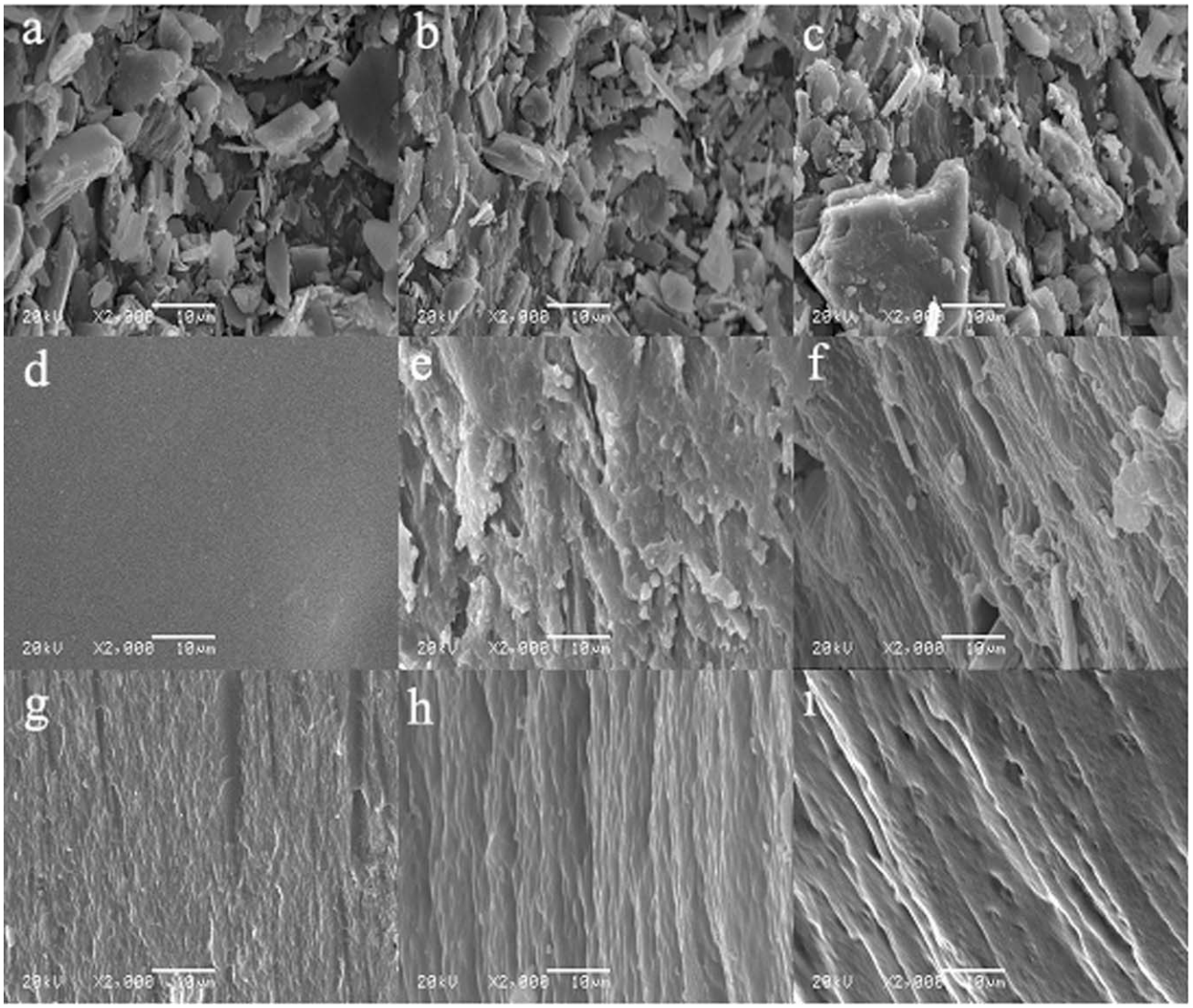

Figure 4 SEM micrographs of (a) K^+-VMT, (b) Mg^{2+}-VMT, (c) Al^{3+}-VMT, (d) GG-*g*-PNaA, (e) GG-*g*-PNaA/Li^+-VMT, (f) GG-*g*-PNaA/K^+-VMT, (g) GG-*g*-PNaA/Mg^{2+}-VMT, (h) GG-*g*-PNaA/Ca^{2+}-VMT, and (i) GG-*g*-PNaA/Al^{3+}-VMT. The content of M^{n+}-VMT in the composite was 5 wt %.

Al^{3+} used to modify VMT on the water absorption was evaluated and is shown in Figure 7. The water absorption of the nanocomposite rapidly increased with increasing concentration of $AlCl_3$ solution from 0.25 to 1.0 mol/L until a maximum was reached. With increasing the concentration of $AlCl_3$ solution, more Al^{3+} could exchange with the other cations on the surface and in the interlayer gallery of VMT. After Al^{3+}-VMT was exfoliated during the reaction, the interlayer Al^{3+} formed more intramolecular and intermolecular complexes with the hydrophilic —COO— groups of the grafted polymer chains.[30] Thus, the polymer network was improved, and the water absorption was improved. However, the excessive concentration of Al^{3+} used to modify VMT may have induced a rapid increase in the effective crosslinking density; this minimized the network space and decreased the water absorption.

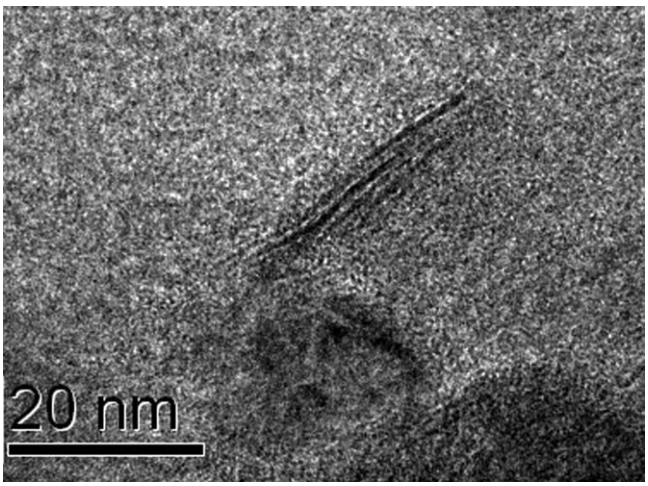

Figure 5 TEM image of the GG-*g*-PNaA/VMT superabsorbent nanocomposite.

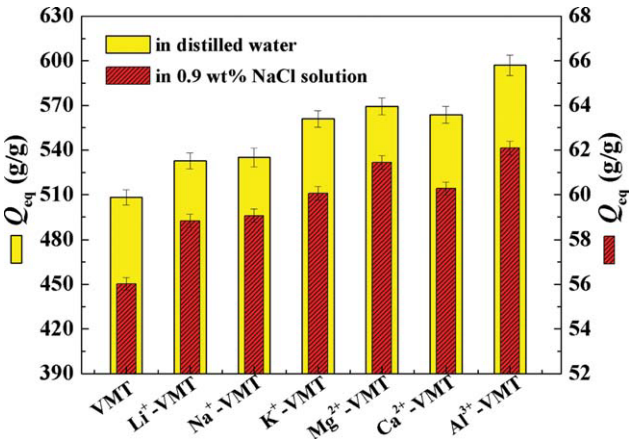

Figure 6 Effects of M^{n+}-VMT on the water absorption in distilled water and a 0.9 wt % NaCl solution. The content of VMT in the composite was 5 wt %. [Color figure can be viewed in the online issue, which is available at wileyonlinelibrary.com.]

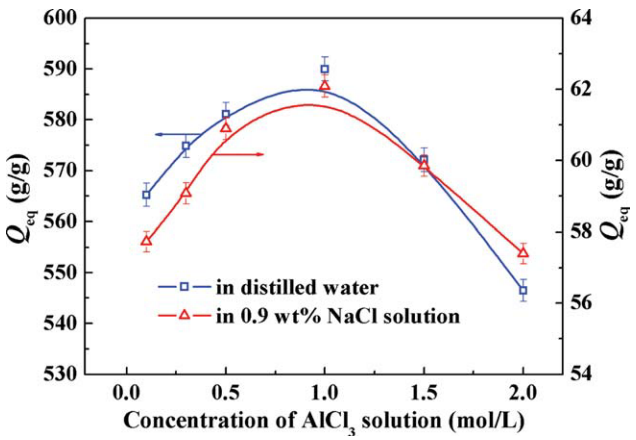

Figure 7 Effects of the $AlCl_3$ concentration on the water absorption in distilled water and a 0.9 wt % NaCl solution. The content of Al^{3+}-VMT in the composite was 5 wt %. [Color figure can be viewed in the online issue, which is available at wileyonlinelibrary.com.]

Effect of the Al^{3+}-VMT content on the water absorption

The alteration of the VMT content in the nanocomposite may have caused the changes in its composition, structure, and swelling properties. As shown in Figure 8, the water absorption of the nanocomposites increased with increasing content of Al^{3+}- VMT and showed a maximum at 5 wt %. It is well known that VMT contains numerous active —OH groups on the edge of the platelet, which can participate in the polymerization reaction by these active groups. Thus, the incorporation of rigid Al^{3+}- VMT prevented the intertwining of grafted polymeric chains and weakened the hydrogen-bonding interaction between —COOH groups. This decreased the degree of physical crosslinking and contributed to the regular formation of the polymer network, and so the water absorption was improved.

However, the excessive addition of VMT may have induced a decrease in the water absorption. This was because the excess platelets of Al^{3+}-VMT physically filled in the network space, which decreased the ratio of hydrophilic groups in the unit volume and the hydrophilicity of the nanocomposite and obscured the network voids for holding water. As a result, the water absorption decreased with increasing VMT content above 5 wt %. A similar tendency was observed for chitosan-*g*-poly(acrylic acid)/organorectorite superabsorbent nanocomposites.[31]

TABLE I
BET Specific Surface Area and the Average Pore Size for the VMT and M^{n+}-VMTs

Sample	BET specific surface area (m^2/g)	Average pore width (4V/A by BET; nm)
VMT	1.6426	8.4652
Li^+-VMT	1.6946	9.3518
Na^+-VMT	2.0965	9.5916
K^+-VMT	3.3075	8.4803
Mg^{2+}-VMT	12.9829	3.3557
Ca^{2+}-VMT	5.8987	6.9822
Al^{3+}-VMT	10.6965	4.7501

Swelling kinetics

Figure 9 shows the kinetic swelling behaviors of composites with certain particle sizes (180–380 μm) in distilled water and a 0.9 wt % NaCl solution. The swelling rate of the composites was higher within 10 min. Later, the swelling rate decreased, and the swelling curves became flatter. The swelling kinetics can be expressed by the Voigt-based viscoelastic model [eq. (2)]:[32]

$$Q_t = Q_\infty(1 - e^{-t/r}) \quad (2)$$

where Q_t is the swelling capability at time t (g/g); Q_∞ is the power parameter (g/g), which denotes the theoretical equilibrium water absorption; t (min) is the time for swelling; and r is the rate parameter (min), which denotes the time required to reach 0.63% of equilibrium water absorption. The experimental data for each sample were fitted by eq. (2) to calculate the values of the parameters r and Q_∞ (Table II). Because r is a measure of the resistance to water permeation, a lower r value may reflect a higher swelling rate.[33] Thus, we concluded that the swelling rate for each sample was in the following order: GG-*g*-PNaA/K^+-VMT in distilled water > GG-*g*-PNaA/raw VMT in distilled water > GG-*g*-PNaA/Mg^{2+}-VMT in distilled water > GG-*g*-PNaA/

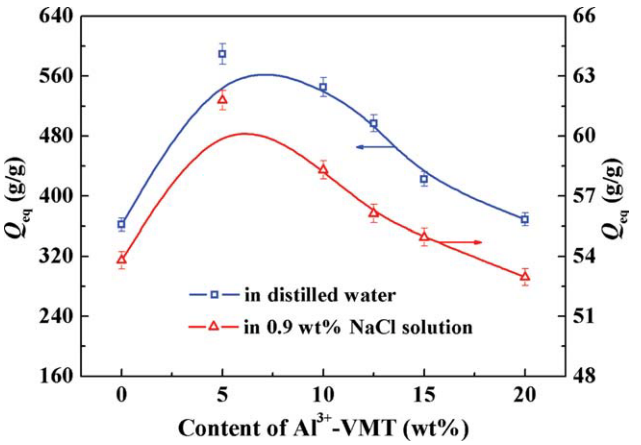

Figure 8 Effect of the Al^{3+}-VMT (Al^{3+} concentration = 1 mol/L) content on the water absorption in distilled water and a 0.9 wt % NaCl solution. [Color figure can be viewed in the online issue, which is available at wiley onlinelibrary.com.]

Al^{3+}-VMT in distilled water > GG-*g*-PNaA/Al^{3+}-VMT in a 0.9 wt % NaCl solution. This result indicates that K^+-modified VMT made a great contribution to the rate, whereas Al^{3+}-modified VMT made a remarkable contribution to the water absorption. The increased concentration of electrolyte in the swelling medium decreased the swelling rate of the superabsorbents.

Effect of the saline solution on the kinetic swelling behavior

The dynamic swelling behaviors of the GG-*g*-PNaA/Al^{3+}-VMT (concentration of Al^{3+} used to modify VMT = 1 mol/L, Al^{3+}-VMT content = 5 wt %) superabsorbent nanocomposite in 2, 5, and 10 mmol/L aqueous solutions of NaCl and $CaCl_2$ were

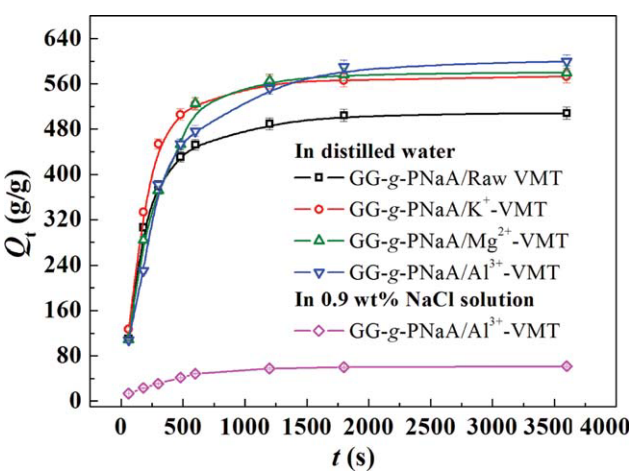

Figure 9 Swelling kinetic curves of the GG-*g*-PNaA/VMT superabsorbent composites in distilled water. [Color figure can be viewed in the online issue, which is available at wileyonlinelibrary.com.]

TABLE II
Swelling Kinetics of the Superabsorbents Containing 5 wt % VMT

Sample	Q_∞ (g/g)	r (s)	R^2
GG-*g*-PNaA/raw VMT	496	209.48	0.9901
GG-*g*-PNaA/K^+-VMT	566	204.73	0.9949
GG-*g*-PNaA/Mg^{2+}-VMT	578	282.74	0.9958
GG-*g*-PNaA/Al^{3+}-VMT	586	324.72	0.9903
	61[a]	393.39[a]	0.9973[a]

[a] Swelling kinetic parameter in a 0.9 wt % NaCl solution.

evaluated and are shown in Figure 10. As shown, the water absorption of the nanocomposite increased with prolonged contact time and reached a swelling equilibrium within 1200 s in the NaCl solution. The equilibrium water absorption of the composite in the saline solution was obviously lower than that in distilled water (Fig. 9), and the water absorption decreased with increasing concentration of saline solution. This may have resulted from the change in the osmotic pressure difference between the gel network and the swelling medium. As described previously,[34,35] the net osmotic pressure (π_{ion}) was determined by Donnan equilibrium theory:

$$\pi_{ion} = RT \sum i(C_i^g - C_i^s) \quad (3)$$

where C_i is the mobile ion concentration of species i and g and s denote the gel and solution phases, respectively. R is the gas constant (0.08206 L atm mol^{-1} K^{-1}, T is thermodynamic (absolute) temperature (K). Because the ion concentration in the gel network (C_i^g) is changeless for a superabsorbent, the increase in the concentration of saline solution (C_i^s) certainly led to a decrease in π_{ion}, which was responsible for the shrinkage of water absorption. However, distinct swelling behaviors were observed in the $CaCl_2$ solution. The water absorption initially increased to 151 g/g (2 mM), 112 g/g (5 mM), and 55 g/g (10 mM) and then decreased until the swelling almost disappeared (Fig. 10). The required time to reach maximum absorption shortened with increasing concentration of the $CaCl_2$ solution. This successive swelling–deswelling process is known as the *overshooting effect*[36] and may have been due to the additional crosslinking action of Ca^{2+} ions due to the interaction with the —COO^- groups of the polymer chains. The FTIR spectra (Fig. 11) showed the change in the chemical environment of —COO^- groups of GG-*g*-PNaA/Al^{3+}-VMT after swelling in NaCl and $CaCl_2$ solutions. The absorption band of the —COO^- groups at 1571 cm^{-1} did not change after swelling in the 5 mM NaCl solution but shifted to 1547 cm^{-1} after swelling in the 5 mM $CaCl_2$ solution.

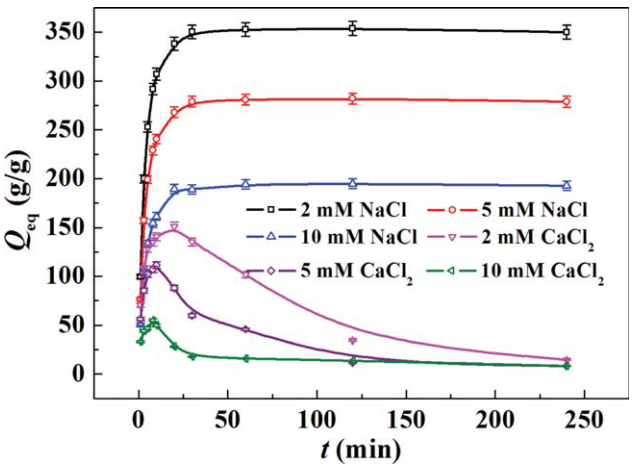

Figure 10 Dynamic swelling curves of GG-*g*-PNaA/Al^{3+}-VMT (Al^{3+} concentration = 1 mol/L, Al^{3+}-VMT content = 5 wt %) in 5 mmol/L NaCl and $CaCl_2$ solutions. [Color figure can be viewed in the online issue, which is available at wileyonlinelibrary.com.]

Effect of the external pH on the kinetic swelling behavior

Figure 12 shows the swelling kinetic curves of the GG-*g*-PNaA/Al^{3+}-VMT (concentration of Al^{3+} used to modify VMT = 1 mol/L, Al^{3+}-VMT content = 5 wt %) nanocomposite in solution with various pH values (2, 3, 7, and 12). The water absorption of the nanocomposite rapidly increased with increasing swelling time until equilibrium was reached under the conditions of pH 7 and 12. However, an obvious overshooting phenomenon was observed when the external pH was equal to 2 or 3.[37] The water absorption rapidly increased to 54 g/g (pH = 2) during the first 5 min and to 294 g/g (pH = 3) during the first 30 min, reached a plateau, and then decreased. The decreasing tendency was more obvious at pH 2 than at pH 3. In acidic medium, the —COO^- group converted to —COOH group, and so its number in the polymeric network decreased. This decreased the electrostatic repulsion among the negatively charged —COO^- groups and restricted the expansion of the polymer network. Also, the increase in the —COOH amount strengthened the intramolecular and intermolecular hydrogen bonding interactions and enhanced the physical crosslinking degree. As a result, the polymer network shrank after it reached maximum expansion under the action of the previous factors. The FTIR spectra (Fig. 11) showed the change in the chemical environment of the —COO^-

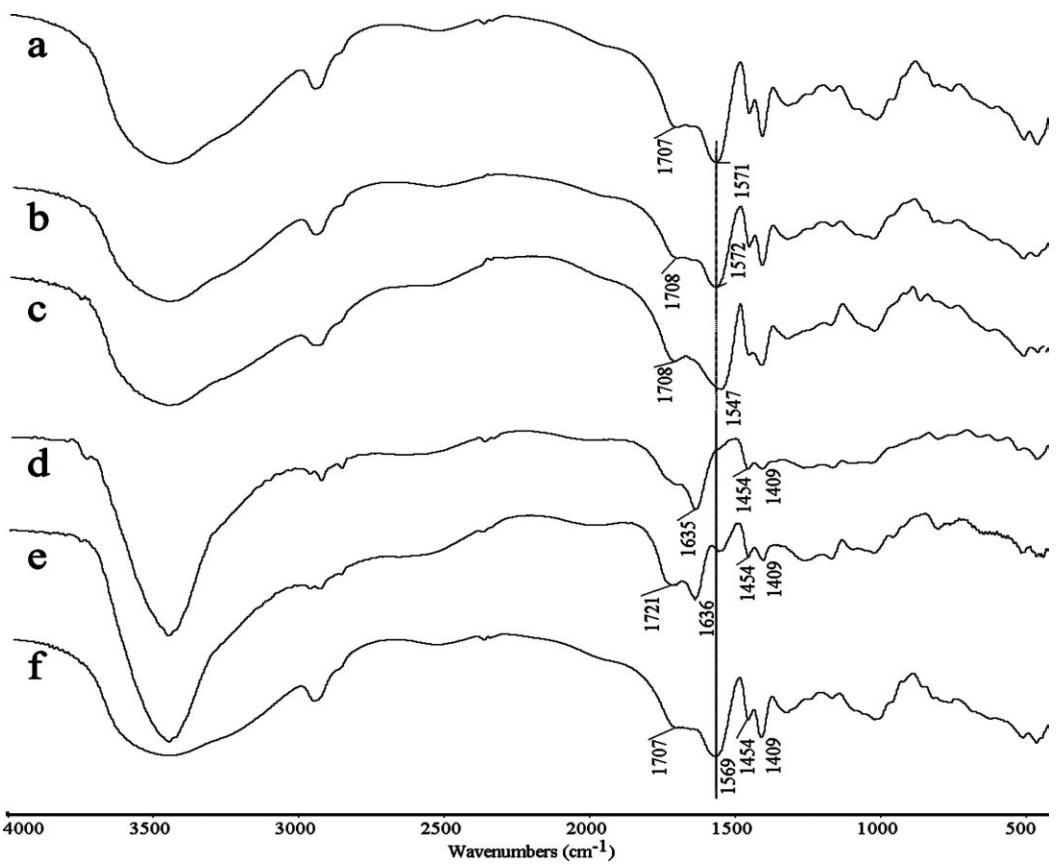

Figure 11 FTIR spectra of (a) GG-*g*-PNaA/Al^{3+}-VMT (Al^{3+} concentration = 1 mol/L and Al^{3+}-VMT content = 5 wt %), (b) the nanocomposite after swelling in a 5 mmol/L NaCl solution, (c) the nanocomposite after swelling in a 5 mmol/L $CaCl_2$ solution, and the nanocomposite after swelling in solutions of (d) pH 2, (e) pH 3, and (f) pH 7.

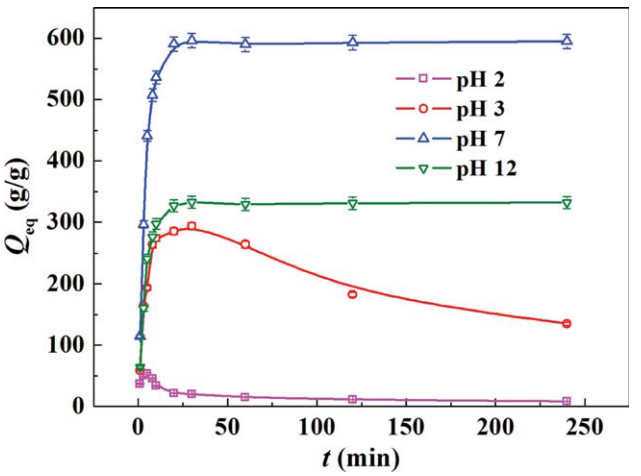

Figure 12 Dynamic swelling curves of GG-*g*-PNaA/Al^{3+}-VMT (Al^{3+} concentration = 1 mol/L and Al^{3+}-VMT content = 5 wt %) in solution with various pH values. [Color figure can be viewed in the online issue, which is available at wileyonlinelibrary.com.]

groups of GG-*g*-PNaA/Al^{3+}-VMT after swelling in solutions at pH 2, 3, and 7. The absorption of the nanocomposite showed no obvious change after swelling in a solution of pH 7 but shifted to high wave numbers (1571–1635 cm^{-1} for pH 2 and 1571–1636 cm^{-1} for pH 3). This indicated the conversion of —COO^- to —COOH and the formation of hydrogen bonds among the —COOH, —OH, and —COO^- groups.

pH-responsive properties

Figure 13 shows the swelling–deswelling behavior of the GG-*g*-PNaA/Al^{3+}-VMT nanocomposite in a 0.1 mol/L buffer solution of phosphate at pH 2 and 7.2.

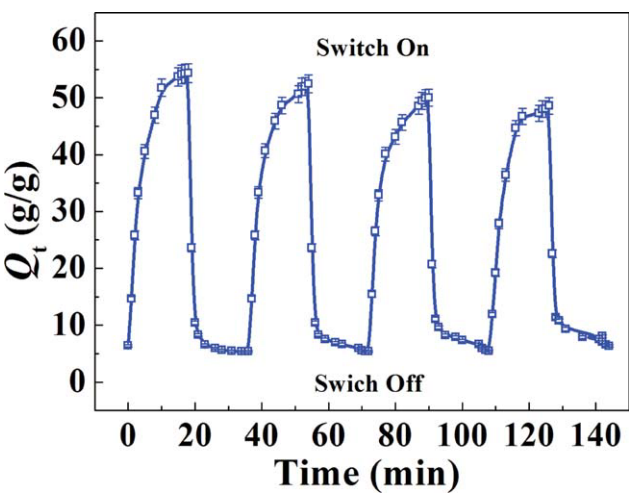

Figure 13 On–off switching behavior of the nanocomposite as reversible pulsatile swelling (pH 7.2) and deswelling (pH 2.0). [Color figure can be viewed in the online issue, which is available at wileyonlinelibrary.com.]

The water absorption was lower at pH 2, but it sharply increased when the external pH increased to 7.2. When the swollen gel at pH 7.2 was immersed in a pH 2 solution, it rapidly shrank because of the protonation of —COO^- groups,[38] and the intriguing on–off switching behavior was observed. After four on–off cycles, the nanocomposite still exhibited better swelling-reversible capabilities, which suggested excellent pH-responsive properties.

CONCLUSIONS

As a continuation of the efforts to reduce the excessive consumption of petroleum-based polymers and the environmental impact resulting from industrial products, GG-*g*-PNaA/M^{n+}-VMT superabsorbent nanocomposites based on natural GG and M^{n+}-VMT were prepared. FTIR, XRD, SEM, and TEM analyses provided evidence that VMT participated in the polymerization reaction through active —OH groups and that M^{n+}-VMT was exfoliated and uniformly dispersed in the GG-*g*-PNaA matrix. Trivalent M^{n+}-VMT enhanced the water absorption to a great extent, and monovalent M^{n+}-VMT made a greater contribution to the swelling rate than VMT. The optimal Al^{3+} concentration for the modification of VMT was 1 mol/L, and the proper VMT content was 5 wt %. The overshooting effects of the developed nanocomposite were observed in multivalent saline solution and acidic pH solutions; this resulted from the complexation of cations with —COO^- groups (chemical action) and the enhancement of hydrogen-bonding interactions among the —COOH groups on the polymer chains (physical action), respectively. In addition, the superabsorbent nanocomposite showed on–off switching behaviors between pH 2 and pH 7.2, and a reversible pH-responsive behavior was observed. The superabsorbent nanocomposites based on renewable and biodegradable natural GG and inorganic M^{n+}-VMT clay exhibited improved water absorption capabilities and rates, overshooting swelling behaviors in saline solution and various pH solutions, and excellent pH-responsive properties. These could be used as potential ecofriendly agricultural water-manageable materials.

References

1. Pavlidou, S.; Papaspyrides, C. D. Prog Polym Sci 2008, 33, 1119.
2. Liu, P. Appl Clay Sci 2007, 38, 64.
3. Utracki, L. A.; Sepehr, M.; Boccaleri, E. Polym Adv Technol 2007, 18, 1.
4. Chu, M.; Zhu, S. Q.; Li, H. M.; Huang, Z. B.; Li, S. Q. J Appl Polym Sci 2006, 102, 5137.
5. Puoci, F.; Iemma, F.; Spizzirri, U. G.; Cirillo, G.; Curcio, M.; Picci, N. Am J Agric Biol Sci 2008, 3, 299.

6. Das, A.; Kothari, V. K.; Makhija, S.; Avyaya K. J Appl Polym Sci 2007, 107, 1466.
7. Sophie, F.; Sophie, F. WO Pat. 024,768 (2006).
8. Guilherme, M. R.; Reis, A. V.; Paulino, A. T.; Fajardo, A. R.; Muniz, E. C.; Tambourgi, E. B. J Appl Polym Sci 2007, 105, 2903.
9. Kaşgöz, H.; Durmus, A. Z.; Kaşgöz, A. Polym Adv Technol 2008, 19, 213.
10. Sadeghi, M.; Hosseinzadeh, H. J. J Bioact Compat Polym 2008, 23, 381.
11. Wang, Q.; Zhang, J. P.; Wang, A. Q. Carbohydr Polym 2009, 78, 731.
12. Demitri, C.; Sole, R. D.; Scalera, F.; Sannino, A.; Vasapollo, G.; Maffezzoli, A.; Ambrosio, L.; Nicolais, L. J Appl Polym Sci 2008, 110, 2453.
13. Sadeghi, M.; Hosseinzadeh, H. J Appl Polym Sci 2008, 108, 1142.
14. Kiatkamjornwong, S.; Mongkolsawat, K.; Sonsuk, M. Polymer 2002, 43, 3915.
15. Wang, W. B.; Wang, A. Q. J Appl Polym Sci 2010, 115, 1814.
16. Pourjavadi, A.; Hosseinzadeh, H.; Sadeghi, M. J Compos Mater 2007, 41, 2057.
17. Zhang, J. P.; Wang, Q.; Wang, A. Q. Carbohydr Polym 2007, 68, 367.
18. Ray, S. S.; Bousmina, M. Prog Mater Sci 2005, 50, 962.
19. Zheng, Y. A.; Li, P.; Zhang, J. P.; Wang, A. Q. Eur Polym J 2007, 43, 1691.
20. Yoon, K. B.; Sung, H. D.; Hwang, Y. Y.; Noh, S. K.; Lee, D. H. Appl Clay Sci 2007, 38, 1.
21. Huang, F. C.; Lee, J. F.; Lee, C. K.; Chao, H. P. Colloids Surf A 2004, 239, 41.
22. Taunk, K.; Behari, K. J Appl Polym Sci 2000, 77, 39.
23. Wu, P. X. J Chin Ceram Soc 2005, 33, 209.
24. Li, A.; Wang, A. Q.; Chen, J. M. J Appl Polym Sci 2004, 92, 1596.
25. Wu, J. H.; Lin, J. M.; Li, G. Q.; Wei, C. R. Polym Int 2001, 50, 1050.
26. Al, E.; Güçlü, G.; İyim, T. B.; Emik, S.; Özgümüş, S. J Appl Polym Sci 2008, 109, 16.
27. Luo, W.; Zhang, W.; Chen, P.; Fang, Y. J Appl Polym Sci 2005, 96, 1341.
28. Handbook of Clay Science: Developments in Clay Science; Bergaya, F.; Theng, B. K. G.; Lagaly G., Eds.; Elsevier: Amsterdam, 2006; Chapter 12.10, Vol. 1, p 984.
29. Slade, P. G.; Stone, P. A.; Radoslovich, E. W. Clays Clay Miner 1985, 33, 51.
30. Zhang, J. P.; Zhao, Y. G.; Wang, A. Q. Polym Eng Sci 2007, 47, 619.
31. Liu, J. H.; Wang, A. Q. J Appl Polym Sci 2008, 110, 678.
32. Kabiri, K.; Omidian, H.; Hashemi, S. A.; Zohuriaan-Mehr, M. J. Eur Polym J 2003, 39, 1341.
33. Pourjavadi, A.; Mahdavinia, G. R. Turk J Chem 2006, 30, 595.
34. Dogu, S.; Kilic, M.; Okay, O. J Appl Polym Sci 2009, 113, 1375.
35. Murthy, P. S. K.; Mohan, Y. M.; Sreeramulu, J.; Raju, K. M. React Funct Polym 2006, 66, 1482.
36. Díez-Peña, E.; Quijada-Garrido, I.; Barrales-Rienda, J. M. Macromolecules 2003, 36, 2475.
37. Yin, Y. H.; Ji, X. M.; Dong, H.; Ying, Y.; Zheng, H. Carbohydr Polym 2008, 71, 682.
38. Lin, J. M.; Tang, Q. W.; Wu, J. H.; Li, Q. H. J Appl Polym Sci 2010, 116, 1376.